

1 **Citation:** Hirt C., W.E. Featherstone, M. Kuhn and S.J. Claessens (2019) Comments on “A high resolution Mars surface  
2 gravity grid” (Górski et al. 2018, Planetary and Space Science 160, 84–106). Accepted for publication in Planetary and  
3 Space Science, 18<sup>th</sup> June 2019, Article PSS4685, doi: 10.1016/j.pss.2019.06.009.  
4

5 **Comments on “A high resolution Mars surface gravity grid” (Górski et al. 2018,**  
6 **Planetary and Space Science 160, 84–106)**  
7

8 C. Hirt<sup>1,2</sup>, W.E. Featherstone<sup>3</sup>, M. Kuhn<sup>3</sup>, and S.J. Claessens<sup>3</sup>

9 <sup>1</sup> Institute for Astronomical and Physical Geodesy, TU Munich, Germany

10 <sup>2</sup> Institute for Advanced Study, TU Munich, Germany

11 <sup>3</sup> School of Earth and Planetary Sciences, Curtin University of Technology, GPO Box U1987, Perth, Australia  
12

13 **Abstract**

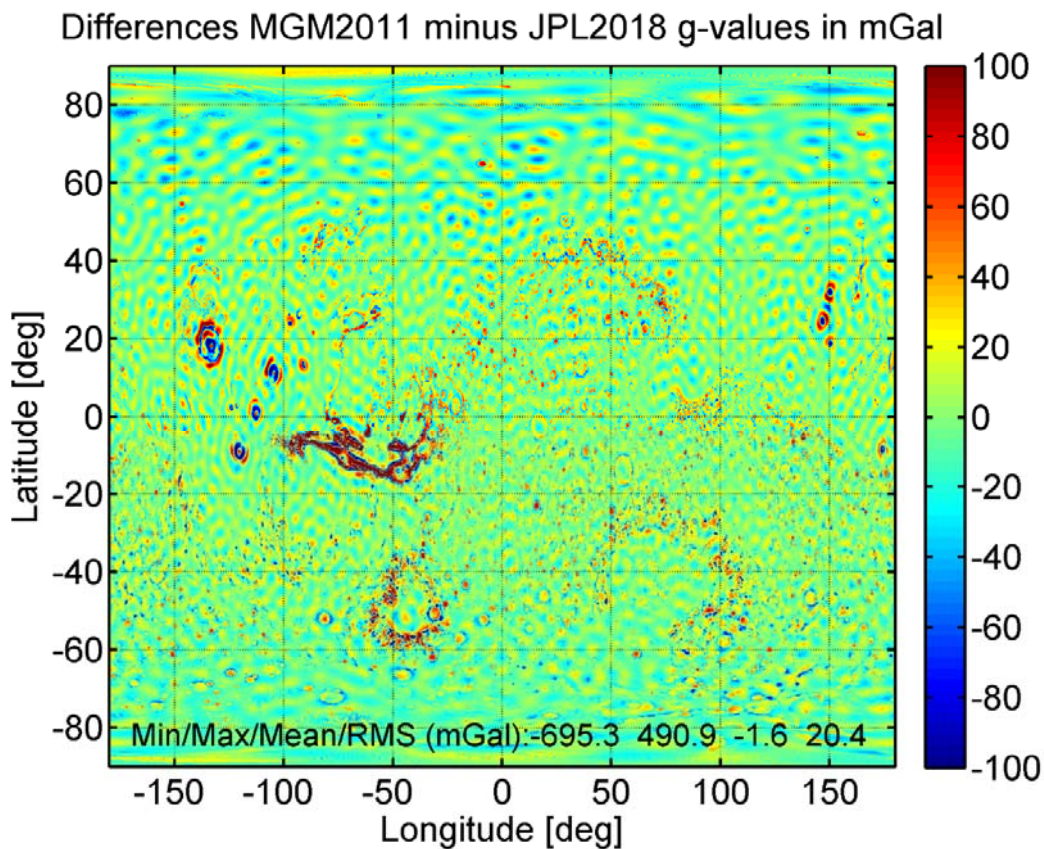
14 Górski et al. (2018, Planetary and Space Science 160, 84–106, doi: 10.1016/j.pss.2018.03.015) developed a  
15 high-resolution surface gravity grid for Mars. They presented a comparison with the Mars Gravity Model  
16 2011 (MGM2011) by Hirt et al. (2012, Planetary and Space Science 67, 147–154. doi:  
17 10.1016/j.pss.2012.02.006), which is based on similar input data, but a different computational  
18 methodology. These two models do not agree very well in their higher-frequency constituents, that is, the  
19 parts related to topography-induced gravity. In the spatial domain, the gravity accelerations from both  
20 models differ by ~20 mGal (root-mean-square) and reach amplitudes as large as ~695 mGal in places. Górski  
21 et al. (2018) suggest that some aspects of the MGM2011 modelling algorithm are “in error”, but without  
22 substantiating this claim nor verifying their model. In this communication, we present results from our  
23 validation experiments using alternative gravity modelling techniques, all showing a close fit with MGM2011,  
24 while being in clear disagreement (to a level of ~40 % of the signal) with the Górski et al. (2018) model. We  
25 discuss and narrow down the origin of the mismatches to a scale-factor of square-root (2), apparently  
26 included in their high-frequency modelling. As a general conclusion, our experiments indicate that the Górski  
27 et al. (2018) model should be treated with some caution, especially over rugged topography so long as the  
28 underlying modelling techniques are not comprehensively validated.  
29

30 **1. Introduction**

31 Górski et al. (2018) describe the development of high-resolution grids of gravitational acceleration  
32 vectors on the surface of Mars, hereafter abbreviated to JPL2018. Together with the Mars Gravity Model  
33 (MGM2011), developed by Hirt et al. (2012a), there are now two gridded data sets available that describe  
34 gravity accelerations (“g-values”) at the topographic surface of Mars with km-level spatial resolution. As  
35 shown in Górski et al. (2018, Fig. 25), g-values from JPL2018 and MGM2011 are not identical. Figure 1 here  
36 illustrates the spatial distribution of the differences, which have a root-mean-square (RMS) value of ~20.4  
37 mGal and frequently exceed 100 mGal, with maximum amplitudes of up to ~695 mGal. Overall, g-values

38 from the two models do not agree very well in many regions, especially those with rugged topography (Fig.  
39 1). The observed discrepancies may be unacceptably large for applications requiring accurate surface g-  
40 values.

41 The purpose of this communication is to present results from our own validation experiments,  
42 clarifying the source of the differences, beyond the considerations made by Górski et al. (2018). We first  
43 summarise relevant similarities and differences among the two models (Sect. 2) before presenting results  
44 from validation experiments (Sect. 3), allowing us to narrow down the origin of the mismatch between the  
45 two models. The findings are discussed and some recommendations given in Sect. 4.  
46



47

48

Fig. 1. Differences between MGM2011 and JPL2018 gravity accelerations.

49

## 50 2. Brief comparison between input data and modelling techniques

51 The JPL2018 and MGM2011 surface g-value models are similarly based on combinations of (1) observed  
52 gravity relying on spacecraft tracking data, coupled with (2) forward-modelled gravity using models of  
53 Martian topography together with some assumed-constant mass-density value. The first component  
54 contributes the long-wavelength part, while the second component represents short-wavelengths that  
55 cannot be sensed by spacecraft orbit analysis due to gravity attenuation with altitude. The basic idea behind  
56 both models – the use of topography-implied (TI) gravity to model the fine structure of the gravitational field

57 – has been used in Earth gravity modelling (e.g., Forsberg and Tscherning 1981) before being adopted in  
58 planetary sciences, to Mars (e.g., Hirt et al. 2012a, Górski et al. 2018) or other planetary bodies. The  
59 underlying assumptions of the MGM2011 forward modelling from geometry only (e.g., 3D variable density  
60 distribution and isostatic compensation) are acknowledged in Hirt et al. (2012a, section 3.3).

61 Both MGM2011 and JPL2018 rely on similar (though not identical) input data sets:

62 (a) Gravity from spacecraft tracking: MGM2011 relies on the MRO110B2 model (Konopliv et al. 2011) to  
63 spherical harmonic degree and order 85, while JPL2018 uses the updated product named MRO120D  
64 (Konopliv et al. 2016) to degree and order 80.

65 (b) Topographic mass models: Both MGM2011 and JPL2018 use global topography from the Mars Orbiter  
66 Laser Altimeter (MOLA) instrument at a 64 pixel per degree spatial resolution (Mission Experiment Gridded  
67 Data Record). Given the similar or identical topography data used, a reasonably good fit among the high-  
68 frequency forward-modelled gravity constituents should be expected, even when using independent  
69 techniques (e.g., Hirt et al. 2016).

70 The first important difference is the adopted uniform topographic mass-density:  $2900 \text{ kg m}^{-3}$  for  
71 MGM2011 and  $2782 \text{ kg m}^{-3}$  for JPL2018. However, this difference is not critical here because it is considered  
72 in our validation experiments (Sect. 2). Even without explicit consideration, the different mass-densities  
73 translate into a scale-factor of less than 5%, so cannot explain differences at the 40% level (cf. Sect. 3). As a  
74 secondary difference, JPL2018 has a higher spatial resolution ( $\sim 1.73 \text{ km}$ ) versus MGM2011 ( $\sim 3 \text{ km}$ ) at the  
75 equator.

76 The third and most significant difference concerns the numerical techniques used for the  
77 computation of g-values from the respective input data:

- 78 • MGM2011 g-values are obtained as sum of three constituents: (1) A reference (“normal”) gravity field  
79 accounts for the gravitational attraction of Mars, as approximated by a rotating ellipsoid of uniform mass-  
80 density, at the 3D field points represented through MOLA topography. (2) MRO110B2 provides the long-  
81 wavelength gravity signals at the MOLA topography. (3) Short-scale gravity signals are forward-modelled  
82 based on the residual terrain modelling (RTM) technique (Forsberg and Tscherning 1981), where a high-  
83 pass filtered topographic mass model is used and cap-limited numerical integration (NI) approximates the  
84 gravity field’s fine structure not captured by (2).
- 85 • In the Górski et al. (2018) approach to determine JPL2018, no reference gravity field is used. Instead of  
86 using RTM, the short-wavelength part is “*derived from convolution of appropriate Green’s functions with*  
87 *the surface mass distribution*”. This approach is based on spherical-harmonic modelling and combines  
88 internal and external topography-generated potentials. The final “*Mars gravity model is represented by a*  
89 *combination of the MRO120D model, truncated at harmonic degree  $n = 80$ , and the topography-derived*  
90 *model for harmonic degrees above  $n = 80$ .*” (Górski et al. 2018).

### 91 3. Comparisons and validation experiments

92 Górski et al. (2018, Fig. 27) harmonically analysed the MGM2011 and JPL2018 g-value grids and  
93 found a drop in spectral energy in MGM2011 w.r.t. JPL2018 near degree 85, that is, at the transition from  
94 observed to TI gravity. Such a drop in spectral energy is absent in the spectrum of JPL2018 around degree 80  
95 (their transition degree). Figure 2 shows our replication of the harmonic analyses as already reported by  
96 Górski et al. (2018), compare the red and blue lines. For the further validations presented here, we have  
97 developed two experimental Mars g-value grids with a methodology independent from the MGM2011 and  
98 JPL2018 methodologies, as follows:

99 1) A model of the external gravitational potential generated by the Martian topography was created  
100 using spherical harmonic analysis of the topography and integer powers thereof (i.e., spectral-domain  
101 gravity forward modelling; e.g., Chao and Rubincam 1989, Hirt et al. 2016) resulting in a topographic  
102 potential model (TPM). Our modelling was limited to degree 250 which is more than sufficient for our  
103 comparison of the discontinuity at degree 85. Note that the adopted degree is low enough to ensure that  
104 series divergence (which can be encountered when evaluating high-degree expansions of gravity field  
105 functionals inside the Brillouin sphere encompassing all planetary mass) is not necessarily a problem. This  
106 was verified by comparing spectral-domain with spatial-domain gravity forward modelling for Mars following  
107 the experimental concepts in Hirt and Kuhn (2017).

108 2) The TPM from step 1 was combined with “observed” MRO spacecraft gravity in the spectral-domain  
109 by merging the coefficients in the following two variants that match MGM2011 and JPL2018 respectively:

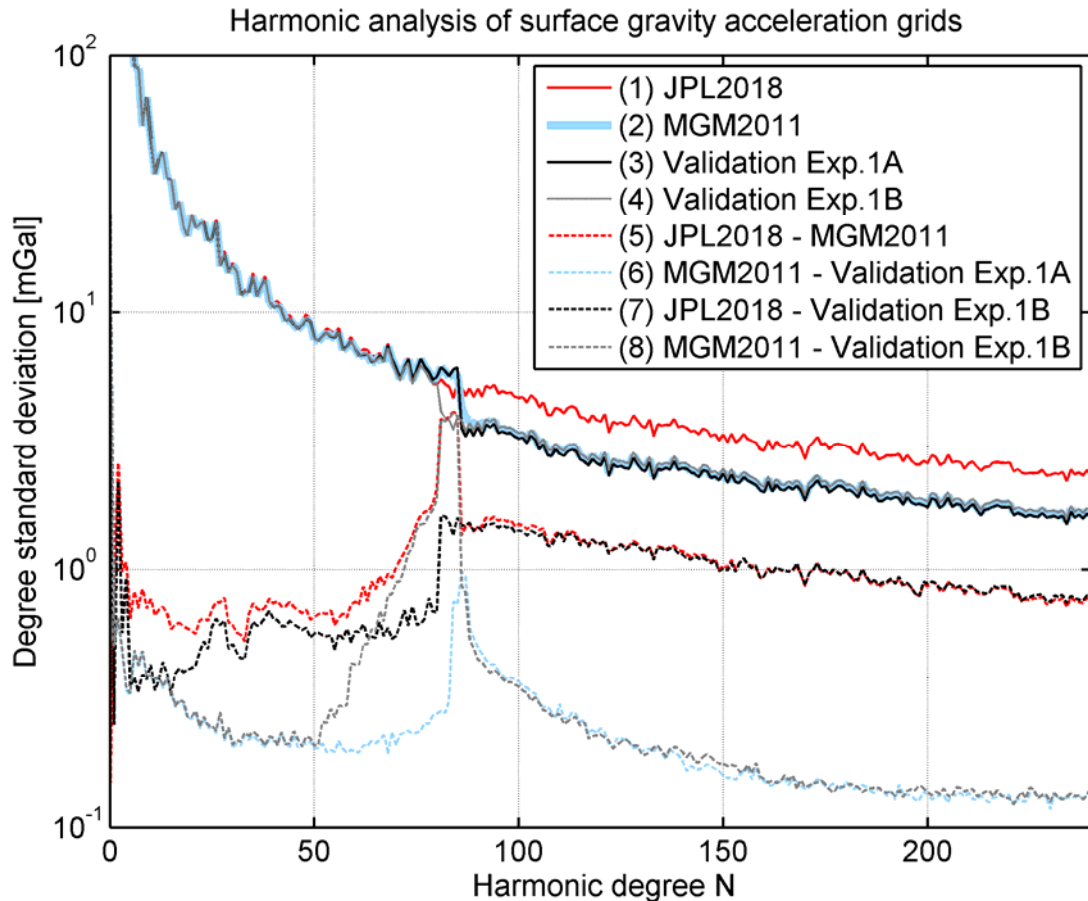
- 110 • Validation model 1A: MRO110B2 ( $N \leq 85$ ) with TPM (density =  $2900 \text{ kg m}^{-3}$  and  $N > 85$ )
- 111 • Validation model 1B: MRO120D ( $N \leq 80$ ) with TPM (density =  $2782 \text{ kg m}^{-3}$  and  $N > 80$ )

112 3) Gravity accelerations  $g$  were computed from the potential coefficients from step 2 at the MOLA 3D  
113 topography using Eq. 121 from Barthelmes (2013).

114 4) Harmonic analysis of the gravity acceleration grid from step 3.

115 This methodology avoids the use of reference gravity fields and RTM forward modelling (as in MGM2011), as  
116 well as the combination of internal/external potentials and Green’s functions (as in JPL2018), so provides an  
117 independent check on the two modelling methodologies.

118 The g-value spectra from these independent validation models are shown in black and grey in Fig. 2,  
119 and differences among the model coefficients in dashed lines. Both validation models are in much closer  
120 agreement with MGM2011 than with JPL2018 for that part of the spectrum where TI information was used  
121 ( $n > 85$ ). This holds regardless of the adopted mass-density. Conversely, JPL2018 mismatches MGM2011 (as  
122 already observed by Górski et al. (2018) and replicated by us), but also with these validation models (black  
123 and red dashed lines in Fig. 2). The mismatch among JPL2018, MGM2011 and the validation models is about  
124 a factor of 1.4 or 40% (in terms of degree standard deviations) or a factor  $\sim 2$  (in terms of degree variances).



125

126 **Fig. 2.** Spectra of gravity accelerations from JPL2018, MGM2011 and two validation models (solid lines) and  
 127 their differences (dotted lines), units in mGal.

128

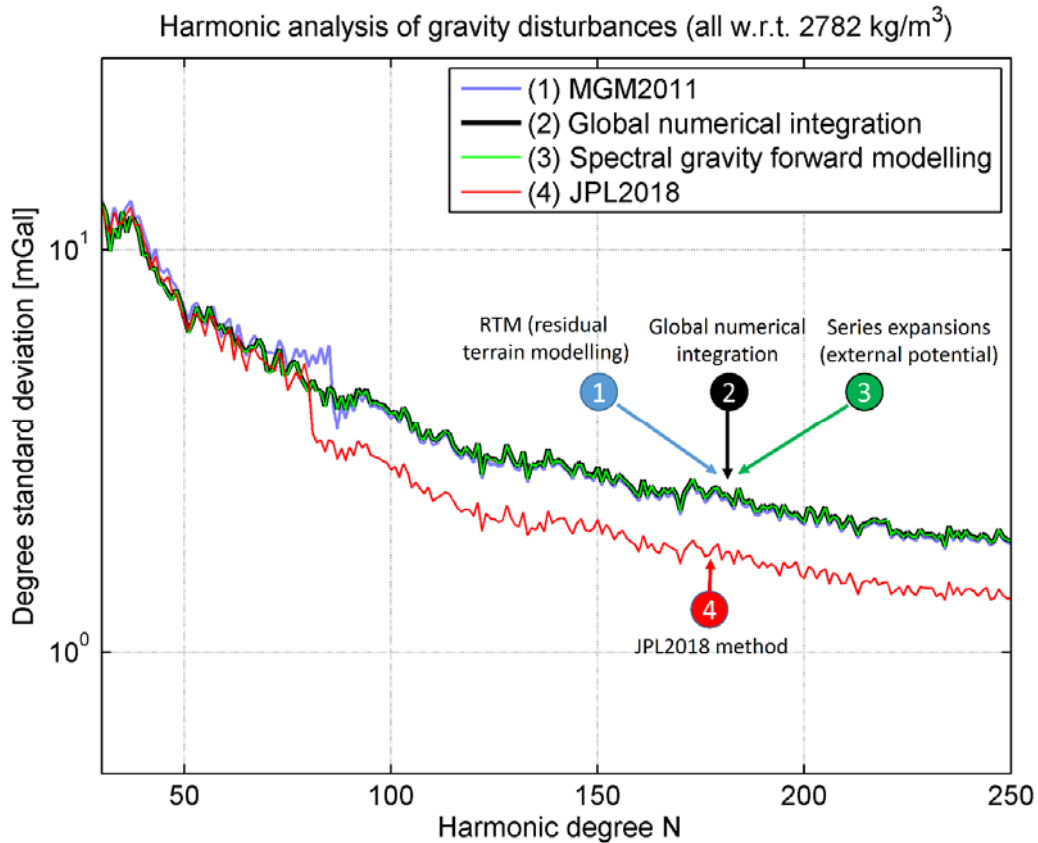
129 We now focus on a comparison of the Mars gravity signal implied by the topographic masses only. By using  
 130 gravity disturbances (i.e., radial derivatives of the topographic potential) instead of gravity accelerations, it is  
 131 possible for us to include another independent validation data set obtained through a global NI.

132 In this approach, Newton's law of gravitation is evaluated in the spatial domain using a combination of  
 133 spherical tesseroids and right-rectangular prisms to represent the topographic mass distribution. Evaluation  
 134 points are located at the 3D MOLA topographic surface and the integration radius is  $180^\circ$  in each case,  
 135 allowing us to recover the full TI gravity signal. The NI is distinct from spectral or RTM techniques, which is  
 136 why it provides an entirely independent check.

137 We include the following four gravity disturbance data sets in this comparison:

- 138 (1) MGM2011 gravity disturbances, as shown in Hirt et al. (2012a, Fig. 3). At short spatial scales,  
 139 MGM2011 relies on the RTM technique,
- 140 (2) Global NI of the MOLA topography at  $0.05^\circ$  spatial resolution using the Newtonian forward-  
 141 modelling integrator by Curtin University,

- 142 (3) Spectral forward modelling, where the gravity disturbances were obtained through gravity syntheses  
 143 of the TPM coefficients (see above) at the 3D MOLA topographic surface, and  
 144 (4) JPL2018, whereby gravity disturbances were obtained through a simple subtraction of the 3D normal  
 145 gravity field (available from the MGM2011 model development, cf. Hirt et al. 2012a, Fig. 2b) from  
 146 the JPL2018 g-value grid.



147  
 148 **Fig. 3.** Spectra of gravity disturbances from JPL2018, MGM2011 and the two validation models “NI” and  
 149 “spectral gravity forward modelling”. The spike visible for MGM2011 near  $n=85$  is a result of the RTM  
 150 filtering problem (see Rexer et al. 2018) together with the MRO110B2 signal structure. It diminishes when  
 151 adopting MRO120D and the Rexer et al. (2018) methods for MGM2011.

152  
 153 For the validation data sets (2) and (3) above, the mass-density of  $2782 \text{ kg m}^{-3}$  was adopted to match that  
 154 used in JPL2018, and the MGM2011 gravity disturbances were scaled to that density value for  $n>85$ . Figure 3  
 155 displays the power spectra obtained through spherical harmonic analysis of the four grids of gravity  
 156 disturbances. MGM2011 (1) is seen to be in close agreement with independent techniques (2) and (3), with  
 157 differences at the level of few percent of the gravity disturbance signal. JPL2018 (4) mismatches any of the  
 158 other three techniques, despite all adopting the JPL2018 mass-density value. The JPL2018 TI gravity  
 159 disturbance signals for  $n>85$  appear to be too small (cf. Fig. 3). A smoother continuation/transition between  
 160 the gravity spectra of the spacecraft-models to the TI components is visible for MGM2011 and the two  
 161 validation data sets, but not for JPL2018.

162 **4. Discussion and concluding remarks**

163 Górski et al. (2018) noted the mismatch between the MGM2011 and JPL2018 g-value spectra, and we  
164 replicate it here. Without providing due evidence, however, Górski et al. (2018, p 101) made the claim:  
165 *“Perhaps the most puzzling feature of this difference is that Hirt et al. used a higher density than we did, but*  
166 *our gravity model has a higher variance value than theirs does. This suggests that some aspects of their*  
167 *algorithm are in error”*, while not taking into consideration or even acknowledging the possibility that the  
168 algorithms or computations behind their own model could equally and legitimately explain the observed  
169 differences.

170 We believe that not only the outcomes of the validation experiments presented in Sect. 3, but also a  
171 MGM2011 replication experiment using Earth as “test laboratory” (Hirt et al. 2012b), when taken together  
172 have verified the validity of the MGM2011 modelling techniques. Also, MGM2011 is based on exactly the  
173 same modelling approach as the GGMplus g-value maps, which have been successfully validated with several  
174 million ground-truth gravity observations around the Earth (Hirt et al. 2013).

175 Our validation experiments show the TI component of JPL2018 to be in mismatch with any of these  
176 three well-established and widely used forward-modelling techniques (RTM, global NI and external spherical  
177 harmonics). To the best of our knowledge, the Górski et al. (2018) modelling technique has not been verified  
178 (well, at least not published in the open literature) with some independent methodology (e.g., NI, tested to  
179 construct an Earth gravity field model that would enable a validation with ground-truth gravity, or some  
180 other independent validation). In light of all this available evidence to us, we do not agree with the above  
181 claim by Górski et al. (2018) and thus defend the veracity of our MGM2011 Martian g-value model.

182 The more intriguing and probably less intuitive feature observed by Górski et al (2018) and shown in  
183 Fig. 2 here is the drop in spectral energy in the MGM2011 gravity acceleration spectrum (as well as in the  
184 validation models), occurring exactly at the transition from spacecraft-observed to TI gravity data. To our  
185 understanding thus far, this drop could be an indication that the gravity-from-topography values neglect  
186 Bouguer gravity signals present in the real (albeit unknown) Martian gravity field, relating to factors such as  
187 3D density variations or isostatic compensation effects. This drop may not be present in case observed  
188 gravity and gravity-from-topography were strongly correlated (near +1) at the transition wavelength. One  
189 possible and plausible explanation for this empirically observed feature can be deduced when decomposing  
190 the spacecraft-topography-combined gravity acceleration model into the gravity effect of the rotating mass-  
191 ellipsoid and that of all contributions residual to it (topographic and all anomalous masses). The following  
192 mechanisms seem to hold:

- 193 • For harmonic degrees  $n > 85$ , no mass-density anomalies are modelled because of the constant mass-  
194 density assumption in the forward modelling for any model. Thus, in case of Mars and in planar  
195 approximation, a normal gradient of  $\sim -0.22$  mGal/m (from the mass-ellipsoid) would directly

196 counteract a Bouguer plate effect of  $\sim 0.12$  mGal/m (topographic masses) in the g-values at short  
197 scales. What can be thought of as a cancellation effect reduces the spectral power of the resulting g-  
198 values, them being the sum of both components.

199 • For  $n \leq 85$ , the models rely on spacecraft gravity observations, so contain field structures generated  
200 by all planetary masses, including the topographic masses and, importantly, all mass-density  
201 anomalies beneath the topography and the planetary interior. In case that substantial mass-density  
202 anomalies exist, the correlation between gravity and topography is lower than +1 (in the present  
203 case, around +0.7 to +0.8, see Hirt et al. 2012a, Fig. 1). As a result, the signal power of the gravity  
204 accelerations increases because of the composite effect of gravity contributions from the mass-  
205 ellipsoid, from the topography and, importantly, also from all mass-density anomalies. A cancellation  
206 effect as described above for  $n > 85$  is therefore not so pronounced.

207 These mechanisms seem to provide some reasonable explanation for the drop in power at  $n=85$ . Of course,  
208 the gravity acceleration spectrum of the real field may naturally not exhibit such a drop. However, it is a  
209 feature to be expected for gravity acceleration *models*, when augmenting a spacecraft model with TI gravity  
210 data at some transition wavelength where gravity and topography are not very closely correlated. Such a  
211 drop can be considered plausible for Mars (gravity-topography-correlation of around +0.8), but it cannot be  
212 expected, e.g., for the Moon, where gravity-topography-correlation is close to +1 at short spatial scales for  
213 modern GRAIL-based gravity models (e.g., Šprlák et al. 2018).

214 To our understanding, the JPL2018 modelling “avoided” the drop in the gravity acceleration  
215 spectrum by determining a best-fitting mass density in the “gravity acceleration space” (Górski et al. 2018,  
216 Eq. 61), which is the most likely cause for the majority of the mismatch with MGM2011 and our two  
217 independent validation models. Due to this aspect of the JPL2018 modelling technique, a smooth transition  
218 from spacecraft to TI gravity was reached (dare we say “forced”) for the gravity acceleration spectrum, but  
219 not for the gravity disturbance spectrum. Any of our validation experiments provide some evidence that this  
220 choice reduces the accuracy of the JPL2018 TI gravity component.

221 Specifically, the mismatch between the topography-implied JPL2018 g-values and our validation  
222 models seems to be a factor of  $\sim 1.4$ , which so happens to be close to the ratio between the mean overall  
223 Martian and crustal density of Mars ( $\sim 3933$  kg m<sup>-3</sup> /  $2782$  kg m<sup>-3</sup>). A closer look at the Górski et al. (2018)  
224 modelling technique shows that gravity acceleration spectra from MRO data and topography were  
225 compared to derive a scale factor of  $\sqrt{2}$  (Górski et al 2018, p 97) that was considered in their algorithm. We  
226 believe that this is a prime candidate to explain the  $\sim 40\%$  signal strength differences between JPL2018  
227 gravity and that of the three comparison data sets (Fig. 3).

228



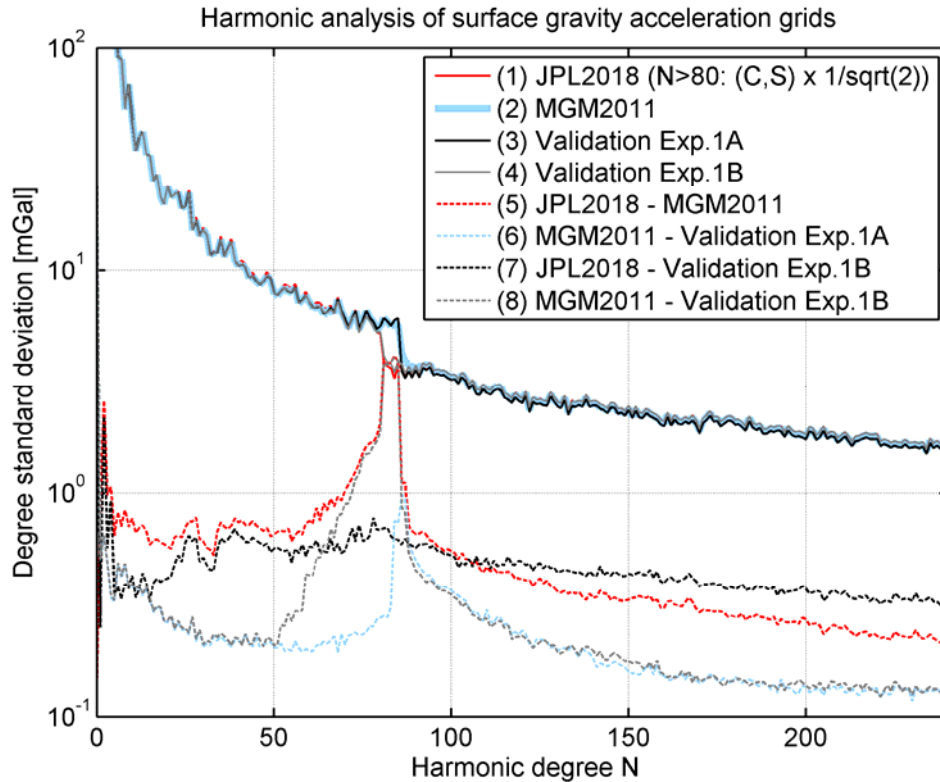


**Fig. 4.** As Fig. 2, but with the JPL2018 coefficients ( $n > 80$ ) re-scaled by a factor of  $1/\sqrt{2}$

As a further test, therefore, we have applied a factor of  $1/\sqrt{2}$  to the JPL2018 coefficients with  $n > 80$ , yielding an improved agreement with MGM2011 and the validation models (see Fig. 4). This appears to corroborate the factor  $\sqrt{2}$  to be chiefly responsible for the mismatch. It is worth noting that the determination of a best-fitting topographic mass-density is usually done by comparing potential coefficients or potential degree variances (e.g., Konopliv et al. 2014).

Finally, we willingly acknowledge that some deficiencies in the MGM2011 modelling technique have become evident over the past years, among them, e.g., a rather simplistic combination of RTM with spacecraft data (also see Fig. 3) or approximation errors in the RTM technique itself (Hirt et al. 2019). These and any further issues should be rectified when developing a next-generation Mars gravity model, e.g., by adopting the RTM technique improvements by Rexer et al. (2018). Nevertheless, these shortcomings in MGM2011 only create errors well below the  $\sim 40\%$  mismatch with JPL2018 observed in Figs. 1, 2 and 3.

As our key conclusion, these and our other validation experiments (Hirt et al. 2012b, Hirt et al. 2013) taken together provide evidence that MGM2011 is not the main contributor to the differences w.r.t. JPL2018. While JPL2018 has been found to be in reasonable agreement with MGM2011 over non-rugged terrain in Górski et al. (2018), spurious differences are encountered over areas with rough topography (also see Fig. 1 here). Over these regions, nevertheless, we recommend that JPL2018 be treated with some caution and scepticism, until the underlying modelling algorithms have been checked and/or verified with some independent methodology.

249 **Acknowledgements**

250 The first author would like to thank JPL for providing their gravity acceleration grid in April 2017 for  
251 evaluation in the role of an external reviewer of NASA's Mars2020 Gravity Model Peer Review. The  
252 validation experiments, results and conclusions presented in this communication were made available to JPL  
253 in May 2017. The computations used in the validation experiments (gravity acceleration and gravity  
254 disturbance grids) will be made available to any interested users upon request.

255 **References**

- 256 Barthelmes, F. (2013) Definition of Functionals of the Geopotential and Their Calculation from Spherical Harmonic Models - Theory and  
257 formulas used by the calculation service of the International Centre for Global Earth Models (ICGEM), Scientific Technical Report  
258 STR09/02, Revised Edition, January 2013. <http://icgem.gfz-potsdam.de/str-0902-revised.pdf>
- 259 Chao BF, Rubincam DP (1989) The gravitational field of Phobos. *Geophysical Research Letters* 16(8): 859-862.  
260 <https://doi.org/10.1029/GL016i008p00859>.
- 261 Forsberg R, Tscherning CC (1981) The use of height data in gravity field approximation by collocation. *Journal of Geophysical Research*  
262 86(B9): 7843-7854. <https://doi.org/10.1029/JB086iB09p07843>.
- 263 Górski KM, Bills BG, Konopliv AS (2018) A high resolution Mars surface gravity grid, *Planetary and Space Science* 160, 84–106.  
264 <https://doi.org/10.1016/j.pss.2018.03.015>.
- 265 Hirt C, Kuhn M (2017) Convergence and divergence in spherical harmonic series of the gravitational field generated by high-resolution  
266 planetary topography – a case study for the Moon. *Journal of Geophysical Research – Planets*, 122(8): 1727-  
267 1746, <https://doi.org/10.1002/2017JE005298>.
- 268 Hirt C, Reußner E, Rexer M and Kuhn M (2016) Topographic gravity modelling for global Bouguer maps to degree 2,160: Validation of  
269 spectral and spatial domain forward modelling techniques at the 10 microgal level. *Journal of Geophysical Research – Solid Earth*  
270 121(9): 6846–6862. <https://doi.org/10.1002/2016JB013249>.
- 271 Hirt C, Claessens SJ, Kuhn M, Featherstone WE (2012a) Kilometer-resolution gravity field of Mars: MGM2011. *Planetary and Space Science*  
272 67(1), 147–154. <https://doi.org/10.1016/j.pss.2012.02.006>.
- 273 Hirt C, Claessens SJ, Kuhn M, Featherstone WE (2012b) Indirect evaluation of Mars Gravity Model 2011 using a replication experiment on  
274 Earth. *Studia Geophysica and Geodetica* 56(4): 957-975. <https://doi.org/10.1007/s11200-011-0468-5>.
- 275 Hirt C, Claessens SJ, Fecher T, Kuhn M, Pail R, Rexer M (2013) New ultra-high resolution picture of Earth's gravity field. *Geophysical Research*  
276 *Letters* 40(16): 4279-4283. <https://doi.org/10.1002/grl.50838>.
- 277 Hirt, C., B. Bucha, M. Yang and M. Kuhn (2019), A numerical study of residual terrain modelling (RTM) techniques and the harmonic  
278 correction using ultra-high degree spectral gravity modelling. *Journal of Geodesy*, doi: 10.1007/s00190-019-01261-x.
- 279 Konopliv AS, Asmar SW, Folkner WM, Karatekin O, Nunes DC, Smerkar SE, Yoder CF, Zuber MT (2011) Mars high resolution gravity fields from  
280 MRO. *Icarus* 211(1): 401–428. <https://doi.org/10.1016/j.icarus.2010.10.004>.
- 281 Konopliv AS, Park RS, Yuan DN, Asmar SW, Watkins MM, Williams JG, Fahnestock E, Kruizinger G, Paik M, Strelalov D, Harvey N, Smith DE,  
282 Zuber MT (2014) High-resolution lunar gravity fields from the GRAIL Primary and Extended Missions. *Geophysical Research Letters*  
283 41(5): 1452-1458. <https://doi.org/10.1002/2013GL059066>.
- 284 Konopliv, AS, Park RS, Folkner WM (2016) An improved JPL Mars gravity field and orientation from Mars orbiter and lander tracking data.  
285 *Icarus* 274, 253–260. <https://doi.org/10.1016/j.icarus.2016.02.052>.
- 286 Rexer M, Hirt C, Bucha B, Holmes S (2018) Solution to the spectral filter problem of residual terrain modelling (RTM). *Journal of Geodesy*  
287 92(6): 675-690. <https://doi.org/10.1007/s00190-017-1086-y>.
- 288 Šprlák, M., S-C. Han and W.E. Featherstone (2018) Forward modelling of global gravity fields with 3D density structures and an application to  
289 the high resolution (~2 km) gravity fields of the Moon. *Journal of Geodesy* 92(8): 847-862. [https://doi.org/10.1007/s00190-017-](https://doi.org/10.1007/s00190-017-1098-7)  
290 1098-7.